Detection efficiency evaluation for a large area neutron sensitive microchannel plate detector *

Yi-ming Wang(王一鸣)[1,2] Yang Tian(田阳)[1,2] Yi-gang Yang(杨祎罡)[1,2;1)] Ren Liu(刘仁)[1,2]
Jing-sheng Pan(潘京生)[3] Xue-wu Wang(王学武)[1,2] Zhi Zhang(张智)[1,2]

[1] Department of Engineering Physics, Tsinghua University, Beijing 100084, China
[2] Key Laboratory of Particle & Radiation Imaging (Tsinghua University), Ministry of Education, Beijing, China
[3] Nanjing Branch, North Night Vision Tech. Co., Ltd., Nanjing 211102, China

Abstract: In this paper, the detection efficiency of a large area neutron sensitive microchannel plate detector has been evaluated. A ^{6}LiF/ZnS scintillator detector 65 mm in diameter and 0.32 mm in thickness, with product code, EJ426HD2, produced by Eljen Technology, was employed as the benchmark detector. The TOF spectra of these two detectors were simultaneously measured and the energy spectra were then deduced to calculate the detection efficiency curve of the ^{n}MCP detector. Tests show the detection efficiency@25.3 meV thermal neutrons is 34% for this ^{n}MCP detector.

Keywords: microchannel plate, neutron detector, detection efficiency

PACS: 28.20.Pr **DOI:** 10.1088/1674-1137/40/9/096004

1 Introduction

Nondestructive Testing (NDT) is of great importance to homeland security, national defense industries and many other areas. Neutron radiography and 2-D neutron imaging techniques are regarded as powerful nondestructive inspecting methods. They have been widely applied in many areas, ranging from the inspection of turbine blades of aircraft engines [1] to the visualization of two-phase flow of operating proton exchange membrane fuel cells [2, 3].

As important NDT techniques, X-ray radiography and gamma-ray radiography have been widely applied in a variety of areas. Compared to X-ray radiography and gamma-ray radiography, neutron radiography has a variety of advantages. Neutrons are much more sensitive to lighter elements, such as hydrogen, carbon and their compounds because neutrons have much larger cross sections for lighter elements than photons. Neutrons are able to penetrate high-Z materials, which are opaque to X-rays. Therefore, neutron radiography can be used for the inspection of hydrogen-containing materials, such as the metal-coated explosives, fluid in the metal container and the hydrides in the metal.

Among various neutron imaging detectors, Neutron-sensitive Micro Channel Plates (^{n}MCP) detectors and related 2-D imaging techniques have played a very important role due to their high spatial resolution. For example, ^{n}MCP detectors have been used for conventional neutron radiography [4], dynamic neutron radiography [5], energy resolved imaging [6], neutron resonance absorption imaging [7] and magnetic field imaging [8]. ^{n}MCP detectors was first proposed by G. W. Fraser et al [9]. Since low energy neutrons have considerable probabilities to be absorbed by a few special nuclides, such as ^{3}He, ^{6}Li, ^{10}B, ^{113}Cd, ^{155}Gd, and ^{157}Gd, normal microchannel plate can be made neutron-sensitive by introducing these nuclides into the normal MCP. Since it was proposed, ^{n}MCP detectors and related 2-D imaging techniques have been used by various researchers to achieve high-quality neutron imaging [10–14]. To expand skill in neutron imaging, a ^{n}MCP detector has been developed. To make the MCP neutron-sensitive, a normal MCP with diameter of 106 mm was doped with 3 mol% of $^{nat}Gd_2O_3$ [15–17]. The delay line anode was used as the readout anode because of its large area, high throughput and good spatial resolution.

Spatial resolution and detection efficiency are two crucial parameters to achieve high-quality neutron imaging for neutron sensitive microchannel plate detectors. The spatial resolution directly determines the quality of the neutron image. The detection efficiency, along with the intensity of the neutron beam, determines the image acquisition time for a neutron imaging detector. To

Received 7 December 2015
∗ Supported by National Natural Science Foundation of China (11375095, 11175098)
1) E-mail: yangyigang@mail.tsinghua.edu.cn

acquire a high-quality neutron image with the microchannel plate detector, enough neutron counts are essential, so adequate statistics of at least ∼100 neutrons per pixel are required [18]. The typical neutron flux of a neutron beam is 10^6-10^7 n/cm$^2\cdot$s [19, 20], the pixel size of the microchannel plate detector is ∼10 μm, the detector's diameter is 106 mm, and the microchannel plate's open area ratio is 56%. So the image acquisition time is estimated to be 7 s to 70 s, with a fully ideal detection efficiency of 100%. However, if the detection efficiency is degraded to 10%, the image acquisition time would be as long as 70 s to 700 s, resulting in a time-consuming imaging process. Hence, it is important to evaluate and improve the detection efficiency to shorten the image acquisition time, in other words, to acquire more effective neutron counts with a given measurement time and to ultimately enhance the quality of the neutron image.

In the previous work, X-ray and neutron images of an USAF-1951 Gd-mask have been acquired with this detector, the spatial resolution has been analysed and the throughput has been evaluated. This detector's spatial resolution is 62 μm for 14 kV X-ray photons and is 88 μm for thermal neutrons respectively [21–24] In this paper, the principle, process and results of the thermal neutron detection efficiency measurement of this detector are presented.

2 The ^{n}MCP detector

The structure of the ^{n}MCP detector is shown in Fig. 1. The detector is composed of a Gd-mask, MCP V-stack, delay-line anode and related electronics. The imaging object (Gd-mask) was designed as the USAF-1951 spatial resolution test chart. The MCP V-stack consists of a neutron sensitive MCP and a normal MCP.

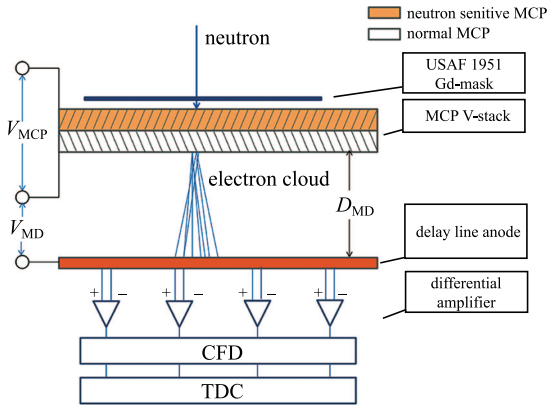

Fig. 1. (color online) Structure of the neutron sensitive MCP detector with delay line readout.

The delay line anode is a two dimensional readout anode with 120 mm by 120 mm area. The 4-channel readout electronics are composed of the differential amplifier, CFD (constant fraction discriminator) and TDC (time to digital converter).

3 Study of the thermal neutron detection efficiency

3.1 Principle and process of the detection efficiency measurement

The detection efficiency measurements were undertaken at the thermal neutron beamline at the CPHS (Compact Pulsed Hadron Source) at Tsinghua University. Considering that the neutron flux of the CPHS would fluctuate and cannot be monitored online precisely, a ^{6}LiF/ZnS scintillator detector 65 mm in diameter and 0.32 mm in thickness, with a product code, EJ426HD2, produced by Eljen Technology, was employed as the benchmark detector. This detector has a detection efficiency of 34%@25.3 meV thermal neutron [25]. The detection efficiency curve of this ^{6}LiF/ZnS scintillator detector was deduced according to neutron capture cross sections of ^{6}Li at different energies. The ^{6}LiF/ZnS detector and the ^{n}MCP detector were placed at two adjacent beamlines of CPHS and the event counts of these two detectors were measured simultaneously. Figure 2 shows the layout of the two detectors.

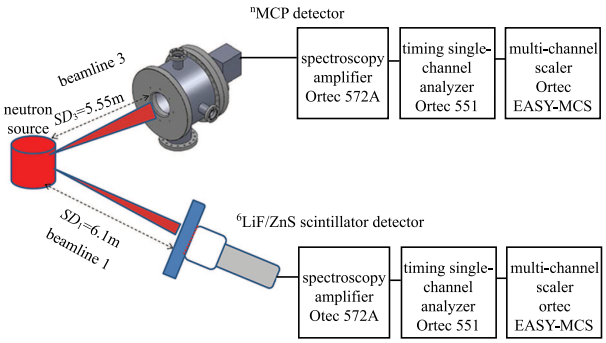

Fig. 2. (color online) Schematic diagram of the neutron detection efficiency measurement setup using the ^{6}LiF/ZnS detector and the ^{n}MCP detector.

The event count ratio of the two detectors can be written as Eq. (1)

$$\frac{n_{^{n}\mathrm{MCP}}}{n_{^{6}\mathrm{Li}}}=\frac{\epsilon_{^{n}\mathrm{MCP}}}{\epsilon_{^{6}\mathrm{Li}}}\left(\frac{SD_{^{6}\mathrm{Li}}}{SD_{^{n}\mathrm{MCP}}}\right)^{2}\frac{S_{^{n}\mathrm{MCP}}}{S_{^{6}\mathrm{Li}}}\frac{1-\tau_{^{n}\mathrm{MCP}}\cdot n_{^{n}\mathrm{MCP}}}{1-\tau_{^{6}\mathrm{Li}}\cdot n_{^{6}\mathrm{Li}}}, \quad (1)$$

where n is the number of event counts, ϵ is the intrinsic detection efficiency of the detector, SD is the distance between the neutron source and the detector, S is the detector's effective detection area, and τ is the detector's dead time. In the measurement, $S_{^{n}\mathrm{MCP}}=33.8$

cm^2(subtracting the Gd-mask's area from the detector's total area), $S_{^6\mathrm{Li}} = 3.14$ cm^2, $SD_{^n\mathrm{MCP}} = 5.55$ m, $SD_{^6\mathrm{Li}} = 6.1$ m and $\tau_{^n\mathrm{MCP}} = \tau_{^6\mathrm{Li}} = 3$ μs, which is determined by the amplifier's time constant for pulse-shaping. With Eq. (1), Eq. (2) can be acquired:

$$\epsilon_{^n\mathrm{MCP}} = 0.0769 \cdot \epsilon_{^6\mathrm{Li}} \cdot \frac{n_{^n\mathrm{MCP}}}{n_{^6\mathrm{Li}}} \cdot \frac{1-\tau_{^6\mathrm{Li}} \cdot n_{^6\mathrm{Li}}}{1-\tau_{^n\mathrm{MCP}} \cdot n_{^n\mathrm{MCP}}}. \quad (2)$$

Based on Eq. (2), the detection efficiencies at different neutron energies can be deduced by measuring the energy spectra of two detectors; hence, the TOF(Time of Flight) spectra of these two detectors were measured. The CPHS worked at pulsed mode and delivered neutrons with a 20 Hz frequency and a 100 μs duration time per period and the measurements were triggered by the synchronization signal of the accelerator.

3.2 Results of the detection efficiency measurement

Figure 3 shows the the TOF spectra of the ^{n}MCP detector and the ^{6}LiF/ZnS detector.

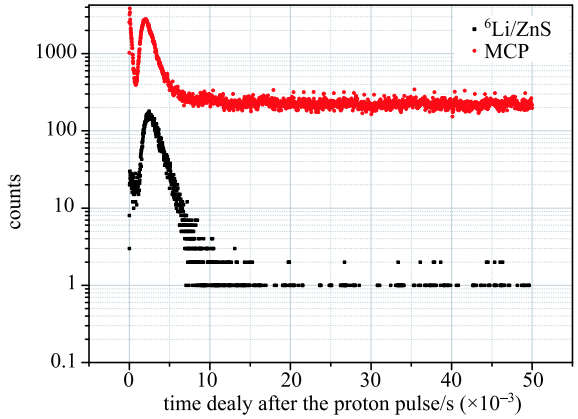

Fig. 3. (color online) TOF spectra of the ^{6}LiF/ZnS detector and the ^{n}MCP detector.

As shown in Fig. 3, there were dark counts in the ^{n}MCP detector's TOF spectrum. To remove the dark counts, the counts with times of flight longer than 15 ms (neutron energies less than 0.71 meV) were removed from the original spectrum. The TOF spectra were transformed as Eq. (3) to the energy spectra.

$$E = \frac{1}{2} \cdot m \cdot \left(\frac{SD}{t}\right)^2, \quad (3)$$

where E is the neutron energy, m is the neutron mass, SD is the distance between the neutron source and the detector and t is the time of flight. The energy spectra of these two detectors can be therefore acquired, as shown in Fig. 4.

According to Eq. (2), the detection efficiency curve of the ^{n}MCP detector can be deduced from the event count ratios of the two detectors and the known detection efficiency curve of the ^{6}LiF/ZnS detector. Fig. 5 shows the calculated detection efficiency curve of the ^{n}MCP detector and the known detection efficiency curve of the ^{6}LiF/ZnS detector. The detection efficiency @25.3meV thermal neutrons is about 34%.

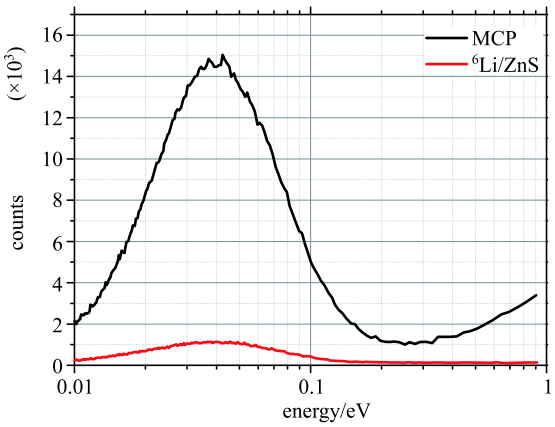

Fig. 4. (color online) Energy spectra of the ^{6}LiF/ZnS detector and the ^{n}MCP detector.

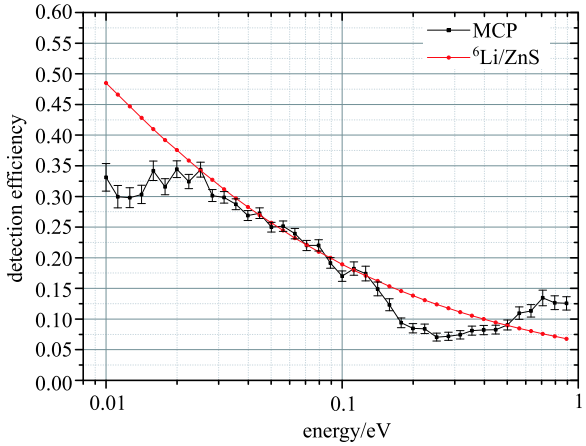

Fig. 5. (color online) Detection efficiency curves of the ^{6}LiF/ZnS detector and the ^{n}MCP detector.

It is important to consider what effect the 100 μs pulse width of the accelerator's synchronizing signal had on the ^{n}MCP detector's detection efficiency measurements. This pulse width introduces a 100 μs error to TOF measurements, and therefore introduces errors to the neutron energy calculation. The relationship between energy error and TOF error is shown in Eq. (4).

$$\mathrm{d}E = m \cdot \left(\frac{SD^2}{t^3}\right) \cdot \mathrm{d}t. \quad (4)$$

Therefore, relative energy errors of the ^{n}MCP detector, $\frac{\mathrm{d}E}{E}$, at different neutron energies can be deduced according to Eq. (4), as shown in Fig. 6.

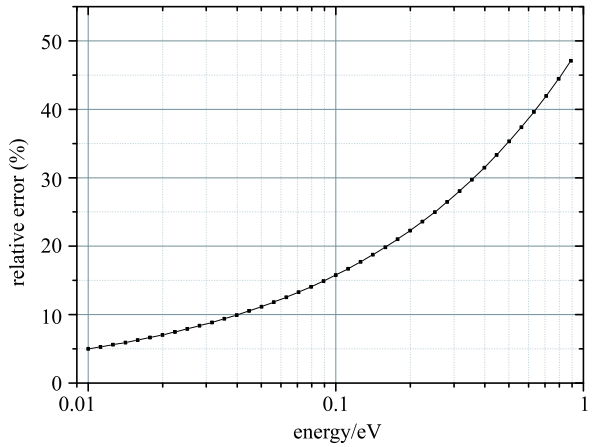

Fig. 6. Relative energy errors at different neutron energies of the ^{n}MCP detector.

Taking neutron energy errors of the ^{n}MCP detector into consideration when drawing detection efficiency curves, Fig. 7 can be acquired, which is the combination of Fig. 5 and Fig. 6.

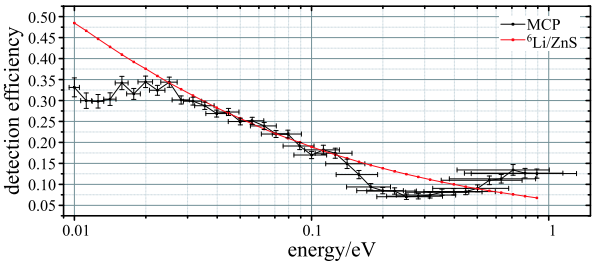

Fig. 7. (color online) Detection efficiency curves of the ^{n}MCP detector and the ^{6}LiF/ZnS detector considering neutron energy error of the ^{n}MCP detector

4 Conclusion and discussion

Previous work on thermal neutron detection efficiency was conducted mainly by A.S. Tremsin et al. The thermal neutron detection efficiency of a ^{n}MCP detector, which consisted of one ^{10}B-doped microchannel plate followed by a stack of two normal MCPs, was measured to be 16% [26], even though the calculation results predict that detection efficiencies of up to 78% are possible [27, 28]. Compared to previous detectors, gadolinium doped microchannel plate detector has higher detection efficiencies for thermal neutrons, as the measurements results showed.

As shown in Fig. 7, there are two regions where the detection efficiencies of the ^{n}MCP detector appear to be relatively lower, one region is near 0.01 eV and the other is near 0.2 eV.

For the region near 0.2 eV, as shown in Fig. 8, the neutron absorption cross section curves of ^{155}Gd and ^{157}Gd suddenly drop at the neutron energy of about 0.05 eV until reaching the neutron energy of ∼1 eV. In this region, the neutron absorption cross section curve of ^{6}Li, however, drops much more slowly than the ^{155}Gd and ^{157}Gd. Due to the relatively small neutron absorption cross sections of ^{155}Gd and ^{157}Gd near 0.2 eV, the measured detection efficiencies of the ^{n}MCP detector are small in this region.

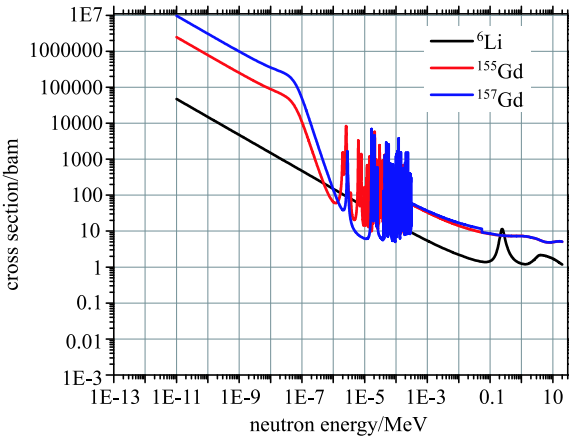

Fig. 8. (color online) Neutron absorption cross sections of ^{155}Gd, ^{157}Gd and ^{6}Li at different neutron energies [29]

For the region near the 0.01 eV, there are several reasons may cause the relatively low detection efficiencies of the ^{n}MCP detector. Firstly, a titanium window with 50 μm thickness was assembled in the front surface of the detector chamber to maintain the vacuum. In addition, an aluminum foil with 100 microns thickness was put in front of the ^{n}MCP to filter the incident UV light from the ion pump that was used to maintain the vacuum. These two pieces of metal will reduce low energy neutrons and will therefore reduce the measured detection efficiencies in the low energy neutrons near 0.01 eV. Secondly, as the TOF spectrum of the ^{n}MCP detector was processed, the dark counts in the ^{n}MCP detector's TOF spectrum were removed. The neutron counts with times of flight longer than 15 ms (neutron energies lower than 0.71 meV) were supposed to be not from the target station and considered as dark counts, since neutrons lower than 0.71 meV are very few in the neutron moderation spectrum of the target station. The dark counts may come from the UV light of the ion pump, ions from the air ionization caused by ion feedback during the electron multiplication in the MCP channels, electrons caused by field emission effect, and α, β radiations caused by the decay of radionuclides in the ^{n}MCP and MCP body. The dark counts were supposed to be constant, therefore every TOF channel was subtracted by the mean value of the neutron counts with times of flight longer than 15 ms and shorter than 50 ms(the longest time of the TOF

spectra). Subtracting dark counts from the ^{n}MCP detector's TOF spectrum may cause errors to the detection efficiency measurements in two ways. On one hand, neutron counts with times of flight between 15 ms and 50 ms are random; on the other hand, no definite conclusion has been drawn at this point regarding whether the neutron counts with times of flight between 15 ms and 50 ms can represent the dark counts with TOF smaller than 15 ms. The neutron beamlines that were used in the measurements are thermal neutron beamlines and the neutron counts near 0.01 eV are very few, so subtracting dark counts in this energy region will cause relatively bigger errors to the ^{n}MCP detector's detection efficiency measurements near 0.01 eV. In summary, the statistical errors of the detection efficiency measurements have been well controlled, as shown in the error bars of Fig. 7. However, since the beamlines that were used in measurements are thermal neutron beamlines and the count rates at the cold neutron region are very few, the detection efficiency measurements at this region will be more noticeably affected by system errors. Relatively, the measured detection efficiencies at energies above the cold neutron energy region are more reliable.

In conclusion, the detection efficiency of a large area neutron sensitive microchannel plate detector has been evaluated through measuring the TOF spectra of the detector and the benchmark detector, a ^{6}LiF/ZnS detector with known detection efficiency curve. The energy spectra were deduced and the detection efficiency curve of the ^{n}MCP detector was calculated. The detection efficiency@25.3 meV thermal neutrons is about 34%, which enable us to conduct neutron imaging experiments at low-intensity neutron beams like the CPHS.

References

1 Cheul Muu Sim, Yi Kyung Kim, TaeJoo Kim et al, Nucl. Instrum. Methods A, **605**: 175 (2009)
2 D. S. Hussey, D. L. Jacobson, M. Arif et al, Journal of Power Sources, **172**: 225–228 (2007)
3 M. A. Hickner, N. P. Siegel, K. S. Chen et al, Journal of The Electrochemical Society, **155** (4): B427–B434 (2008)
4 A. S. Tremsin, J. B. McPhate, J. V. Vallerga et al, Nucl. Instrum. Methods A, **652**: 400 (2011)
5 A. S. Tremsin, M. J. Mühlbauer, Burkhard Schillinger et al, IEEE Trans. Nucl. Sci., **57**: 2955–2962 (2010)
6 A. S. Tremsin, J. B. McPhate, J. V. Vallerga et al, IEEE Sensors Journal, **11** (12): 3433–3436 (2011)
7 A. S. Tremsin, J. B. McPhate, J. V. Vallerga et al, IEEE Nuclear Science Symposium Conference Record, **N30-5**: 1501–1505 (2011)
8 N. Kardjilov, I. Manke, M. Strobl et al, Nature Phys., **4**: 399–403 (2008)
9 G. W. Fraser, J. F. Pearson, Nucl. Instrum. Methods A, **293**: 569 (1990)
10 O. H. W. Siegmund, J. Vallerga, A.S. Tremsin et al, Nucl. Instrum. Methods A, **576**: 178 (2007)
11 A. S. Tremsin, J. V. Vallerga, J. B. McPhate et al, Nucl. Instrum. Methods A, **592**: 374 (2008)
12 A. S. Tremsin, J. B. McPhate, J. V. Vallerga et al, Nucl. Instrum. Methods A, **605**: 140 (2009)
13 O. H. W. Siegmund, J. V. Vallerga, A. S. Tremsin et al, IEEE Trans. Nucl. Sci., **NS-56** (N3): 1203 (2009)
14 A. S. Tremsin, Neutron News, **23** (4): 35 (2012)
15 J. Pan, Y. Yang, Y. Tian et al, J. of Instrum, **8**: P01015 (2013)
16 Nianhua Lu, Yiang Yang, Jingwen Lv et al, Physics Procedia, **26**: 309–316 (2012)
17 Nianhua Lu, Yiang Yang, Jingwen Lv et al, Physics Procedia, **26**: 61–69 (2012)
18 A. S. Tremsin, J. B. McPhate, J. V. Vallerga et al, Nucl. Instrum. Methods A, **628**: 415 (2011)
19 D. S. Hussey, D. L. Jacobson, M. Arif et al, Nucl. Instrum. Methods A, **542**: 9 (2005)
20 A. Hilger, N. Kardjilov, M. Strobl et al, Physica B, **385–386**: 1213 (2006)
21 Yiming Wang, Yigang Yang, Xuewu Wang et al, Nucl. Instrum. Methods A, **784**: 226 (2015)
22 TIAN Yang, YANG Yi-Gang, Pan Jing-Sheng et al, Chinese Physics C, **38** (08): 086003 (2014)
23 TIAN Yang, YANG Yi-Gang, LI Yu-Lan et al, Chinese Physics C, **37** (05): 056001 (2013)
24 TIAN Yang, YANG Yi-Gang, LI Yu-Lan et al, Chinese Physics C, **36** (04): 339–343 (2012)
25 http://www.eljentechnology.com/index.php/products/neutron-detectors/113-ej-426
26 A. S. Tresmin, J. B. McPhate, J. V. Vallerga et al, Nucl. Instrum. Methods A, **604**: 140 (2009)
27 Anton S. Tremsin, W. Bruce Feller, R. Gregory Downing, Nucl. Instrum. Methods A, **539**: 278 (2005)
28 A. S. Tremsin, W. Bruce Feller, R. Gregory Downing et al, IEEE Trans. Nucl. Sci., **NS-52** (N5): 1739 (2005)
29 http://www.nndc.bnl.gov/exfor/endf11.jsp, Arp 14th, 2016